HHS Public Access

Author manuscript

Nat Struct Mol Biol. Author manuscript; available in PMC 2016 April 01.

Published in final edited form as:

Nat Struct Mol Biol. 2015 October ; 22(10): 815–823. doi:10.1038/nsmb.3097.

Synaptotagmin-1 binds to PIP_2-containing membrane but not to SNAREs at physiological ionic strength

Yongsoo Park[1], **Jong Bae Seo**[2], **Alicia Fraind**[6], **Angel Pérez-Lara**[1], **Halenur Yavuz**[1], **Kyungreem Han**[7], **Seung-Ryoung Jung**[2], **Iman Kattan**[4], **Peter Jomo Walla**[4,5], **MooYoung Choi**[7], **David S. Cafiso**[6,*], **Duk-Su Koh**[2,3,*], and **Reinhard Jahn**[1,*]

[1]Department of Neurobiology, Max-Planck-Institute for Biophysical Chemistry, Göttingen, Germany.

[2]Department of Physiology and Biophysics, University of Washington, Seattle, Washington, USA.

[3]Department of Physics, Pohang University of Science and Technology, Pohang, Kyungbuk, Republic of Korea.

[4]Research Group Biomolecular Spectroscopy and Single-Molecule Detection, Max Planck Institute for Biophysical Chemistry, Göttingen, Germany.

[5]Department of Biophysical Chemistry, Institute for Physical and Theoretical Chemistry, University of Braunschweig, Braunschweig, Germany.

[6]Department of Chemistry, the Center for Membrane Biology, University of Virginia, Charlottesville, Virginia, USA.

[7]Department of Physics and Astronomy and Center for Theoretical Physics, Seoul National University, Seoul, Republic of Korea.

Abstract

Ca^{2+}-sensor synaptotagmin-1 is thought to trigger membrane fusion by binding to acidic membrane lipids and SNARE proteins. Previous work has shown that binding is mediated by electrostatic interactions that are sensitive to the ionic environment. However, the influence of divalent or polyvalent ions, at physiological concentrations, on synaptotagmin binding to

*Corresponding authors: David S. Cafiso, Department of Chemistry, the Center for Membrane Biology, University of Virginia, Charlottesville, Virginia, USA. Phone: (434) 924-3067, Fax: (434) 924-3567, cafiso@virginia.edu. Duk-Su Koh, Department of Physiology and Biophysics, University of Washington, Seattle, Washington, USA. Phone: (206) 543-6661; Fax: (206) 685-0619; koh@uw.edu. Reinhard Jahn, Department of Neurobiology, Max-Planck-Institute for Biophysical Chemistry, Göttingen, Germany, Phone: x49-551-201-1635; Fax: x49-551-201-1499; rjahn@gwdg.de.

Author Contributions:

Y.P. designed and performed most biochemical and biophysical study including fusion assay, FRET, floatation assay, and anisotropy. Y.P. collected and analyzed data. J.B.S. under the supervision of D.S.K. carried out dual-recording of amperometry and patch-clamping. A.F. and D.S.C. performed DEER. K.H., M.Y.C., and S.R.J. developed mathematical model and performed numerical simulation. A.P.L. carried out stopped-flow spectroscopy. I.K. under supervision of P.J.W. performed FCCS. H.Y. assisted with protein labeling. Y.P., K.H., M.Y.C., D.S.C., D.S.K., and R.J. wrote the manuscript. All authors read and provided their comments on the draft. D.S.C., D.S.K., and R.J. supervised the project.

Competing financial interests:

The authors declare no competing financial interests.

membranes or SNAREs has not been explored. Here we show that binding of rat synaptotagmin-1 to membranes containing PIP_2 is regulated by charge shielding caused by the presence of divalent cations. Surprisingly, polyvalent ions such as ATP and Mg^{2+} completely abrogate synaptotagmin-1 binding to SNAREs regardless of whether Ca^{2+} is present or not. Altogether, our data suggest that at physiological ion concentrations Ca^{2+}-dependent synaptotagmin-1 binding is confined to PIP_2-containing membrane patches in the plasma membrane, suggesting that membrane interaction of synaptotagmin-1 rather than SNARE binding triggers exocytosis of vesicles.

Neurotransmitters contained in synaptic vesicles and secretory granules are released by exocytotic membrane fusion in response to an elevation of intracellular Ca^{2+}. Soluble *N*-ethylmaleimide-sensitive factor attachment protein receptor (SNARE) proteins are considered to be the fusion machinery[1,2]. Q-SNAREs (syntaxin-1 and SNAP-25) localized in the plasma membrane assemble with an R-SNARE (synaptobrevin-2, also called VAMP-2) in the vesicle membrane, thereby bringing the vesicle and plasma membranes into close proximity and initiating membrane merger[3].

Synaptotagmin-1, anchored in the vesicle membrane, is one of the main Ca^{2+} sensors mediating fast Ca^{2+}-dependent vesicle fusion. Synaptotagmin-1 consists of two Ca^{2+}-binding C2 domains[4], referred to as the C2A and C2B domains, respectively, that interact with acidic phospholipids upon Ca^{2+} binding[5–7]. In addition to the Ca^{2+}-binding loops, the C2B domain contains a polybasic region, enriched with lysine residues[8] that interacts with phosphatidylinositol 4,5-bisphosphate (PIP_2)[9,10]. Recent evidence suggests that syntaxin-1A clusters PIP_2, which interacts with the polybasic region in C2B domain, thereby positioning synaptotagmin-1 at the site of fusion before arrival of the Ca^{2+} stimulus[11,12]. PIP_2 binds to and directly controls the activity of multiple proteins such as ion channels and pumps[13,14]. The inositol head group of PIP_2 is highly charged due to three negative phosphates and therefore generates a strong negative local electrostatic potential[15]. In aqueous solution, the negative potential attracts cations and forms an ‘ion cloud’ or ‘double layer’ that was first recognized by Helmholtz in 1853[16] . This ionic double-layer accounts for many surface phenomena including the behavior of colloids and other surfaces in contact with aqueous solutions[17,18].

In addition to acidic phospholipids and PIP_2, synaptotagmin-1 directly binds to SNARE proteins syntaxin-1 and SNAP-25 and to SNARE complexes containing these SNAREs. Binding is observable both in native extracts using immunoprecipitation and pulldown approaches and *in vitro* using purified proteins. Binding can be measured in the absence of Ca^{2+} but is accelerated by Ca^{2+}, and it appears to be mediated mainly by the polybasic region of the C2B domain[19–22]. Molecular dynamics simulations suggest that multiple acidic residues of syntaxin-1A (E224, E228, D231 and E234) and the acidic residues on SNAP-25A (D51, E52 and E55) may interact with the basic residues of the C2B domain in synaptotagmin-1[23].

The molecular mechanisms by which synaptotagmin-1 triggers exocytosis are poorly understood and highly debated[2]. This is primarily due to the fact that it is very difficult to integrate the diverse binding modes of synaptotagmin-1 observed *in vitro* under variable

experimental conditions into a coherent molecular pathway towards fusion that is compatible with physiological data. In most models, the synaptotagmin-1/SNARE complex interaction plays a critical role and is thought to be directly responsible for the dramatic acceleration by Ca^{2+}-ions of synaptic vesicle exocytosis. Despite this emerging consensus, it has been very difficult to pinpoint the effect of synaptotagmin-1 binding on the SNARE conformational cycle and its relationship to membrane fusion. Both inhibitory and activating effects of synaptotagmin-1 on SNARE assembly have been postulated but neither the nature of synaptotagmin-SNARE binding nor the effects of binding on SNARE function are understood at the molecular level.

Intriguingly, synaptotagmin-1 binding to both acidic phospholipids and SNARE proteins is highly sensitive to the presence of electrolytes, indicating that electrostatics plays a major role in these interactions. For instance, Ca^{2+}-independent binding of synaptotagmin-1 to PIP_2 is reduced by Mg^{2+} ions[24]. Moreover, we have recently shown that ATP and other polyphosphates, at physiological concentrations, reduce binding to acidic phospholipids[25]. Similarly, binding of synaptotagmin-1 to SNAREs and the SNARE complexes, which has been investigated in many studies from different laboratories[26,27], appears to be exquisitely sensitive to the ionic strength of the medium, being barely detectable at physiological ion concentrations, e.g. 150 mM NaCl or KCl[28,29].

For these reasons, we set out to shed light on the interactions of synaptotagmin-1 with SNARE proteins and membrane lipids in the presence of divalent and polyvalent ions in a physiologically relevant concentration range. Our data show that the affinity of synaptotagmin-1 to its binding partners is reduced by multivalent ions. Whereas Ca^{2+}-dependent synaptotagmin-1 binding to PIP_2-containing membranes persists at physiological concentrations of monovalent ions, Mg^{2+}, and ATP, synaptotagmin-1 binding to SNAREs is not measurable under these conditions, regardless of whether Ca^{2+} is present or whether the SNAREs are embedded in a membrane containing acidic phospholipids. We conclude that synaptotagmin-1 triggering requires specific binding to acidic membrane lipids, in particular PIP_2 clusters at the base of SNARE proteins. In contrast, our data do not support models involving a direct effect on SNARE zippering by synaptotagmin-1 binding to SNAREs.

Results

PIP_2 shielding by Mg^{2+} reduces Ca^{2+}-dependent fusion

It is well established that binding of synaptotagmin-1 to the membrane lipid PIP_2 plays an important role in Ca^{2+}-dependent vesicle fusion[25,30–32]. Because cations such as Mg^{2+} electrostatically interact with the negatively charged head groups of PIP_2[33] and reduce the PIP_2 availability in the plasma membrane by shielding its negative charge[34], we tested whether Mg^{2+} interferes with the binding of synaptotagmin-1 during Ca^{2+}-enhancement of SNARE-dependent vesicle fusion *in vitro*. To this end, we used an *in vitro* fusion assay involving fusion between purified chromaffin granules (CGs) containing endogenous synaptobrevin-2 and proteoliposomes containing a stabilized Q-SNARE acceptor complex (together with acidic phospholipids; 1% PIP_2 and 10% phosphatidylserine, PS)[3,25]. Ca^{2+} at 80 ~ 100 μM potently accelerated CG fusion (caused by an interaction between synaptotagmin on CGs and PIP_2 in the acceptor liposome[25]) whereas inclusion of soluble

synaptobrevin-2 ($Syb_{1–96}$) blocked the fusion, indicating that fusion is SNARE-dependent (Fig. 1a). Intriguingly, Mg^{2+} inhibited Ca^{2+}-dependent CG fusion in a dose-dependent manner, with a complete inhibition of Ca^{2+}-dependent enhancement at 10 mM $MgCl_2$ (Fig. 1a,b). This result correlates well with a former study showing that nonphysiologically high Mg^{2+} concentrations (> 5 mM) reduced Ca^{2+}-dependent exocytosis in chromaffin cells[35,36].

To test whether the Mg^{2+} effect is caused by an inhibition of synaptotagmin-1 binding to PIP_2, we monitored the binding of synaptotagmin-1 to the membrane at different Mg^{2+} concentrations. A soluble fragment of synaptotagmin-1 including both C2 domains (residues 97–421, termed C2AB fragment) was labeled with Alexa Fluor 488 so that the binding of C2AB fragment to PIP_2-containing liposomes results in the increase of fluorescence anisotropy due to a reduction of the mobility (see Online Methods for details). Millimolar Mg^{2+} reduced Ca^{2+}-dependent C2AB binding to PIP_2-containing liposomes (Fig. 1c,d), thus paralleling the fusion experiments.

Biphasic regulation of Ca^{2+} on CG fusion

Electrostatic shielding is primarily determined by the valence and concentrations of counterions[17,18], raising the possibility that not only Mg^{2+} but also Ca^{2+} at nonphysiologically high concentrations (mM range) shields PIP_2. Ca^{2+} promoted *in vitro* vesicle fusion with the maximum at a concentration of around 80 μM[25] and higher concentrations of Ca^{2+} progressively reduced Ca^{2+}-dependent fusion, with complete inhibition at 10 mM, resulting in a bell-shaped dose-dependence (Fig. 2a). A similarly biphasic response to Ca^{2+} was observed on exocytosis of chromaffin cells. Cultured rat chromaffin cells were perfused with varying Ca^{2+} concentrations using patch electrodes and carbon fiber amperometry[37]. Increase of free Ca^{2+} concentrations enhanced spike frequency up to around 200 μM and then declined, being abolished above 4 mM (Fig. 2b), verifying the biphasic effect of Ca^{2+} on vesicle fusion. Note that the inhibitory effect of high Ca^{2+} concentrations was observable during the entire recording time after breaking through the membrane, excluding burst-like fast release at the beginning, associated with pool depletion.

To confirm that charge shielding of PIP_2 by elevated Ca^{2+} concentrations reduces binding of synaptotagmin-1, we repeated the binding experiments shown in Fig. 1c,d for Ca^{2+}. We again observed a bell-shaped curve (Fig. 2c). Intriguingly, C2AB binding only declined at concentrations above 1 mM, reminiscent of the dose-response curve of Mg^{2+} shown in Fig. 1d, but clearly different from the Ca^{2+} dose-response of fusion both *in vitro* and in chromaffin cells (Fig. 2a,b). This discrepancy may be explained by considering that synaptotagmin-1 not only binds in *trans* to the PIP_2-containing target membrane, but also shows Ca^{2+}-dependent *cis*-binding to acidic phospholipids in its resident (CG) membrane[25]. Since these two binding activities are expected to compete with each other, we also measured binding of synaptotagmin-1 to CGs (Fig. 2d). The result again shows a bell-shaped curve but as previously reported[25] binding required higher Ca^{2+} concentrations (above 0.5 mM), probably due to the fact that the CGs do not contain PIP_2. Note that even high concentrations of cations had no effect on the anisotropy signal in the absence of membranes. (Supplementary Fig. 1a).

Synaptotagmin-1 also binds to PIP_2 independently of Ca^{2+}, which is mediated by an electrostatic interaction with the positively charged polybasic region within the C2B domain of synaptotagmin-1[11,24,30,38,39]. We therefore tested whether Ca^{2+}-independent binding is also reduced upon charge shielding by cations. Effective binding requires higher PIP_2 concentrations (5%) whereas no substantial binding was detected when the membrane contained only 1% PIP_2 (Supplementary Fig. 1b,c). As expected, addition of liposomes containing 5% PIP_2 to labeled C2AB fragments resulted in binding (Supplementary Fig. 2a–c), which was mediated by the polybasic region. Importantly, high concentrations of $MgCl_2$ reduced Ca^{2+}-independent C2AB binding to PIP_2-containing liposomes in a dose-dependent manner (Supplementary Fig. 2d,e).

To better estimate the contribution of PIP_2 shielding by divalent cations, we built a mathematical model (see Online Methods for details), which considers the accumulation of divalent cations due to the local potential generated by PIP_2 and the resulting reduction of free PIP_2 available for synaptotagmin-1 binding. This model can successfully fit *trans*- and *cis*-interactions of C2AB fragment (Fig. 1d, Fig. 2c,d) at different Mg^{2+} and Ca^{2+} concentrations, supporting our hypothesis that divalent cations at several millimolar concentrations electrostatically shield PIP_2. The model explains that the fusion rate drops between 100 μM and 1 mM Ca^{2+} due to substantial increase of inhibitory *cis*-interaction (Fig. 2d) and fusion continues to decrease between 1 and 10 mM Ca^{2+}, resulting from both increase of *cis*-binding and decrease of *trans*-binding of synaptotagmin-1 (Fig. 2c,d).

Finally, our hypothesis predicts that cations with higher charge density than divalent cations are more effective in shielding the negative charges of PIP_2. In fact, spermine (+4) as well as neomycin (+6) inhibited Ca^{2+}-triggered exocytosis at lower concentrations than divalent cations (Supplementary Fig. 3a,b).The only deviation from the model was the observation that Ca^{2+}-triggered exocytosis was higher with 15 mM Mg^{2+} than 1 mM Mg^{2+} (Supplementary Fig. 3b). We consider this unexpected result in Discussion.

Taken together, the data show that the activity of synaptotagmin-1 can be modulated by divalent cations, which can be readily explained by the charge shielding effect of these cations on acidic phospholipids and PIP_2. Our previous observations[25] showed that polyanions such as ATP also inhibit synaptotagmin-1 binding to acidic membrane lipids (mainly PS) although, again, Ca^{2+}-dependent binding to PIP_2 persists. Thus, charge shielding by polyvalent ions affect both binding partners: acidic membrane lipids, in particular PIP_2, are shielded by divalent cations whereas the polybasic region of synaptotagmin-1 is shielded by polyvalent anions including ATP. In confirmation of the latter, we also showed that ATP indeed binds directly to the polybasic region of synaptotagmin-1 using a FRET-based assay (Supplementary Fig. 4).

Ion-dependence of synaptotagmin-1 binding to SNAREs

Synaptotagmin-1 binding to SNARE proteins is considered to be at least as relevant for triggering exocytosis as binding to membrane lipids. Again, binding was previously shown to be sensitive to the salt concentration[28,29], suggesting that it is primarily driven by electrostatic interactions between basic residues of synaptotagmin-1 and acidic residues of SNAP-25 and syntaxin-1A that are exposed on the surface of the SNARE complex, a notion

that has recently been confirmed and extended based on NMR-experiments and modeling[23]. However, so far it has not been tested to which extent and with which affinity the SNARE-synaptotagmin-1 interaction is preserved under physiological ionic conditions, i.e. when not only monovalent but also divalent and polyvalent ions are present such as Mg^{2+} and ATP.

For these reasons, we investigated how the interaction between synaptotagmin-1 and SNAREs is affected by Mg^{2+}/ATP. First, we employed double electron-electron resonance (DEER)[40,41] to characterize the association between synaptotagmin-1 and the SNARE complex in solution using spin-labeled variants of the C2AB domain and a ternary SNARE complex lacking the membrane anchor domains. Three single cysteine mutants of the syntaxin-1A H3 segment and nine mutants of a soluble fragment of C2AB fragment were generated to introduce a single spin-label side chain (R1), thereby producing 27 different spin pairs for the C2AB-SNARE complex (Fig. 3a). Under normal ionic strength conditions (140 mM KCl, 12 mM NaCl, pH=7.2) without polyvalent ions, the dipolar interactions between spin-pairs are weak and the distance distributions are highly heterogeneous, yielding distance distributions that differ by 30 Ångstroms or more. These data indicate that there are multiple binding modes for the C2AB-SNARE complex that involve primarily the C2B domain and the C-terminal end of the SNARE complex (Fig. 3b and Supplementary Fig. 5a). Models that are available for this interaction from smFRET (ref. [28]) and MD simulation (ref. [23]) capture the extremes in the distributions (Fig. 3b and Supplementary Fig. 5a,c), but even the multiple MD models fail to capture the structural heterogeneity seen by DEER. When the physiological concentration range[42–44] of Mg^{2+}/ATP (2 mM) were added, the already weak intramolecular dipole signal was virtually eliminated, indicating that the heterogeneous interaction between synaptotagmin-1 and the SNARE is prevented by charge shielding of basic residues in the C2B domain (Fig. 3c). As a control, R1 spin labels within the SNARE complex yield strong dipolar interactions and distances that match predictions based upon the structure (Supplementary Fig. 5b).

The experiments described above were carried out using soluble protein fragments, and it is conceivable that binding is enhanced when the SNAREs are anchored in the membrane. Therefore, we prepared liposomes containing a membrane-anchored ternary SNARE complex using SNAP-25A labeled with Texas Red at the position 130C. The C2AB fragment ($Syt_{97–421}$) was labeled with Alexa Fluor 488 at 342C close to the polybasic region of C2B domain[31], allowing for monitoring binding by FRET (Fig. 4a–d). In the first set of experiments, no acidic phospholipids were incorporated into the liposomes. When these liposomes were mixed with the labeled C2AB fragment in a low ionic strength buffer (50 mM KCl), donor emission was quenched and enhanced by 1 mM Ca^{2+}, confirming that under such conditions direct binding does occur[19,20,28,29,45,46] (Fig. 4a). In contrast, binding was dramatically reduced when the experiment was carried out at a KCl concentration of 150 mM regardless of whether the ternary SNARE complex (Fig. 4b) or syntaxin-1A (Supplementary Fig. 6a–d) is incorporated, again in agreement with previous reports[28,29].

Addition of Mg^{2+} and ATP at moderate concentrations (1 mM and 3 mM, respectively) completely abolished the interaction of C2AB fragment with the SNARE complex already at 50 mM KCl (Fig. 4c,d), and this did not change when syntaxin-1A instead of a ternary SNARE complex was used (Supplementary Fig. 6a–d). Binding was not restored by the

addition of 1 mM Ca^{2+} (Fig. 4d and Supplementary Fig.6c,d). Similarly, addition of purified complexin II which is thought to modulate synaptotagmin-1-SNARE interactions failed to restore binding (Supplementary Fig. 6e–h). To exclude that binding does occur but is not reported by the FRET pair, we measured binding between synaptotagmin-1 and liposome by flotation gradients. Again, binding of C2AB fragment to SNARE-containing liposomes was abolished when physiological ionic conditions were used (Supplementary Fig. 7a).

While results above show that synaptotagmin-1 does not bind to SNARE complexes under physiological ionic conditions, we cannot exclude that synaptotagmin-1 binding to membranes containing acidic phospholipids and PIP_2 results in a high local concentration and/or a preferred orientation in the vicinity of membrane-anchored SNAREs, thus facilitating SNARE binding. To test for this possibility, we reconstituted the SNARE complex in liposomes containing 10% PS and 1% PIP_2 (Fig. 5). Ca^{2+} induced a FRET signal between synaptotagmin-1 and the SNARE complex (Fig. 5a). This FRET signal could result from (i) direct binding of C2AB to SNAREs or (ii) close proximity (but no direct binding) due to the recruitment of C2AB to PIP_2 surrounding syntaxin-1A clusters[12]. To differentiate between these possibilities, we carried out a competition experiment in which either excess amount of soluble unlabeled SNARE complex or excess amounts of protein-free liposomes containing PS and PIP_2 were added after induction of the Ca^{2+}-dependent FRET signals. Whereas addition of protein-free liposomes reversed the FRET signals in a dose-dependent manner, no effect was observed when SNARE complexes were added (Fig. 5b). These data suggest that synaptotagmin-1 does not directly bind to the surface of SNARE complexes, but to PIP_2-containing acidic membranes in the vicinity of SNAREs. For further confirmation, we compared the binding kinetics of synaptotagmin-1 to PS- and PIP_2-containing liposomes that either contained SNARE complexes or were free of protein in the presence of 100 μM Ca^{2+}, again in the physiological ionic conditions, i.e. 150 mM KCl, 1 mM $MgCl_2$, and 3 mM ATP. If the SNARE complexes contribute to the membrane recruitment of C2AB to the PIP_2-containing membrane, an enhancement of the binding rate is expected. Binding kinetics was measured by FRET between the C2AB fragment and a labeled membrane lipid (rhodamine-phosphatidylethanolamine, Rho-PE) using a stopped-flow setup (Fig. 6a). No difference was found between the two sets of liposomes (Fig. 6b,c), demonstrating that the presence of SNAREs does not contribute to the membrane binding of C2AB. To rule out that membrane-anchored full-length synaptotagmin-1 behaves differently with respect to SNARE binding we reconstituted synaptotagmin-1 into liposomes and estimated binding by monitoring docking between the two vesicle populations using fluorescence cross-correlation spectroscopy[47]. Again, binding to SNARE containing liposomes devoid of acidic lipids was reduced close to background levels in the presence of physiological salt concentrations and Mg^{2+}/ATP both in the absence or presence of Ca^{2+}-ions whereas Ca^{2+}-dependent binding was observable to liposomes containing PS and PIP_2 (Supplementary Fig. 7b,c, see also Ref.[47]). We conclude that synaptotagmin-1 binds to membranes containing acidic lipids but not to SNAREs in a physiological ionic environment.

Discussion

In this study, we have investigated the electrostatic nature of synaptotagmin-1 binding to membranes and SNARE proteins in a physiological ionic environment. In the absence of Ca^{2+}, binding to both SNAREs and membranes is abolished. In the presence of Ca^{2+}, synaptotagmin-1 specifically binds to PIP_2-containing membranes, rendering it likely that it is this interaction that is mainly responsible for triggering exocytosis. Our results strongly confirm the notion that synaptotagmin-1 operates as an electrostatic switch, which was first proposed by Rizo and colleagues[48]. The electrostatic component clearly dominates membrane binding both in the absence and the presence of Ca^{2+}, with the latter being supported by the fast kinetics of synaptotagmin-1 binding and unbinding (Perez-Lara et al., unpublished observations).

Binding of synaptotagmin-1 to membranes is governed by long-range Coulombic interactions that are modulated both by the ionic strength of the medium and by the absorption of cations to the interface. This charge shielding by the counter ions of PIP_2 depends on the local potential generated by PIP_2, bulk concentrations of the counter ions, and the ionic strength of the solution, as predicted by our mathematical modeling (Supplementary Fig. 7d and Supplementary Table 1). Importantly, the intracellular concentrations of divalent and polyvalent ions are in a range where shielding is just beginning to become significant: cations including spermine (+4) are in the millimolar range[49], free Mg^{2+} ranges between 0.5 and 3 mM[43,44], and intracellular ATP concentrations range between 1 and 10 mM[42]. This agrees well with our observation that spermine and neomycin (+6) suppress exocytosis in chromaffin cells at low mM concentrations (Supplementary Fig. 3b). Intriguingly, the only exception is Mg^{2+} (Supplementary Fig. 3b). We consistently observed increase of exocytosis even with 15 mM Mg^{2+}, which was shown to abolish C2AB-PIP_2 binding and vesicle fusion *in vitro*. Currently the reason for this is not clear but it is conceivable that one or several steps preceding vesicle exocytosis in intact cells are promoted by millimolar concentrations of Mg^{2+}, thus compensating for the shielding effect.

Our data show that the affinity of the synaptotagmin-1-SNARE interaction is reduced beyond detection at physiological ionic conditions, questioning its physiological relevance for regulating exocytosis. Several structural models have been proposed that are based upon NMR[50], pseudocontact shifts and MD simulations[23], mass spectrometry[51] and single-molecule FRET[28], revealing quite different views of the predicted conformational structure of the complex. For the NMR and MD-based models, there is close association between the charged polybasic face of C2B and the SNARE complex, but for the FRET-based model it appears that regions opposite the membrane binding loops are in contact with the SNAREs. Importantly, our DEER data strongly support that the interaction between synaptotagmin-1 and SNAREs are heterogeneous and non-specific (Fig. 3b and Supplementary Fig. 5a). First, in every case the distributions are extremely broad. These data indicate that a single structure does not exist for the synaptotagmin-1-SNARE interaction and that there is likely a configuration where the polybasic face of C2B approaches close to the SNAREs and those where it does not. Secondly, addition of Ca^{2+} produces only slight changes in the distributions and does not substantially alter the complex that is formed. Thirdly, a direct

comparison between the predictions of the FRET-based model[28], MD based models[23], and the distributions observed by EPR can be made and is shown by the histograms in Fig. 3b and Supplementary Fig. 5. In general, distances predicted by the FRET-based model[28] capture the long distance end of the DEER distance distribution, while the MD-based models often reproduce the shorter end of the distribution. Finally, it should be noted that these DEER data are completely consistent with an earlier study using continuous wave EPR, indicating that the synaptotagmin-1-SNARE interaction is structurally heterogeneous[52] and they also explain why pseudocontact shifts for C2B bound to Dy^{3+}-labeled SNAREs are highly averaged[23]. We conclude that the interaction of synaptotagmin-1 with the surface of the SNARE complex is predominantly electrostatic. The association of these proteins may be dominated by one conformation under certain low ionic strength conditions; however, this does not appear to take place at equilibrium under more normal conditions. It is hard to imagine that such a low energy synaptotagmin-1-SNARE interaction has any major influence on SNARE zippering and thus on the kinetics of exocytosis[53].

Figure 7 summarizes the synaptotagmin-1 binding activities that are measurable at different ionic conditions in the absence and presence of Ca^{2+}. Clearly, the only Ca^{2+}-triggered binding event that is high affinity under physiological ionic conditions, and might contribute sufficient energy to overcome activation energy barriers, is to PIP_2-containing membranes. In the absence of Ca^{2+}, synaptotagmin-1 binding seems to be occurring only at high PIP_2 concentrations (higher than 5%[11]), and we also observed reduced but measurable binding at high PIP_2-concentrations under physiological ionic conditions (unpublished observations). Considering that PIP_2 forms microdomains in which PIP_2 is highly enriched (up to 84%)[12], and does so preferably at the base of SNARE complexes, it is conceivable that significant Ca^{2+}-independent binding takes place at such PIP_2 microdomains.

In summary, our data demonstrate that electrostatic charge shielding by cations, multivalent cations, and ATP profoundly interferes with the various binding activities of synaptotagmin-1, explaining why the binding properties of synaptotagmin-1 reported in the literature are highly variable. Importantly, our data do not support an interaction of synaptotagmin-1 with SNARE proteins at physiological ionic conditions regardless of whether Ca^{2+} is present or not, thus shifting the focus on the PIP_2 interaction as the physiologically relevant binding event. This leaves two possibilities for the synaptotagmin-1-mediated trigger event of exocytosis. First, binding perturbs the local lipidic environment, thus reducing the energy barrier needed to be overcome for membrane merger. Such perturbation could either be mainly confined to the membrane surface or the molecule may penetrate deeper into the hydrophobic core of the bilayer. At the surface, synaptotagmin-1 may alter the local distribution of charged lipids (de-mixing)[54] at the base of the SNAREs, and this effect may be enhanced by Ca^{2+}. Such a mechanism would be in accordance with the primarily electrostatic nature of binding. On the other hand, side-chains of membrane-bound synaptotagmin-1 were previously shown to establish hydrophobic interactions with the bilayer core, with Trp residues “snorkeling” at the hydrophilic-hydrophobic boundary[30], and this may have effects on overall bilayer structure. Indeed, synaptotagmin-1, at least when added at saturating concentrations, was shown to deform

membranes by inducing local curvature stress[55,56], which is featured as causative for exocytosis triggering in several models (see e.g. [57]).

Second, synaptotagmin-1 may trigger exocytosis by shortening the distance between the membranes, thus triggering SNARE nucleation and/or zippering. This view is supported by the observation that synaptotagmin-1 is capable of cross-linking membranes, and that upon Ca^{2+}-binding the membrane distance is shortened[58]. The latter concept has recently been challenged by the topology of docked and primed synaptic vesicles as measured by high-pressure freezing and cryo-EM tomography[59] since the distance between the vesicle and plasma membrane was found to be below 2 nm, not leaving much room for further shortening. Clearly, more work will be required before the mechanism of calcium triggering by synaptotagmin is unraveled.

Online Methods

Materials

2Na-ATP was purchased from AppliChem (Darmstadt, Germany). Neomycin and spermine were from Sigma (St Louis, MO). Alexa Fluor 647-labeled ATP and BODIPY TR-labeled ATP were from Invitrogen (Carlsbad, CA). All other chemicals were reagent grade and obtained from standard suppliers. All lipids are from Avanti Polar lipids (Alabaster, AL) except of Oregon Green-DHPE and Texas Red-DHPE (Invitrogen).

Purification of chromaffin granules (CGs)

As described elsewhere[25], CGs were purified from bovine adrenal medulla by continuous sucrose gradient centrifugation as the last purification step. CGs were resuspended in 120 mM K-glutamate, 20 mM K-acetate, and 20 mM HEPES, pH 7.4 adjusted with KOH.

Protein purification and protein labeling

All SNARE and C2AB constructs were based on *Rattus norvegicus* sequences, expressed in *E. coli* strain BL21 (DE3), and purified by Ni-NTA affinity chromatography followed by ion-exchange chromatography. The stabilized Q-SNARE acceptor complex consisting of syntaxin-1A (aa 183–288), SNAP-25A (aa 1–206, no cysteine), and a C-terminal synaptobrevin-2 fragment (aa 49–96) was purified as described earlier[3]. The Q-SNARE complex containing full-length syntaxin-1A (1–288) and SNAP-25A (no cysteine) was purified after co-expression[25,61]. The Q-SNARE complex and stabilized Q-SNARE complex were purified by ion-exchange chromatography on Mono Q column (GE Healthcare, Piscataway, NJ) in the presence of 50 mM n-octyl-β-D-glucoside. The C2AB fragment of synaptotagmin-1 (97–421), and the KAKA mutant (K326A, K327A) were purified by Mono S column (GE Healthcare, Piscataway, NJ) as described previously[31,62]. Point mutated C2AB (S342C) was labeled with Alexa Fluor 488 C5 maleimide[31]. A single cysteine SNAP-25A mutant (Cys130) was labelled with Texas Red C5 bromoacetamide. The ternary SNARE complex consisting of syntaxin-1A (183–288), labeled SNAP-25A (Cys130), and synaptobrevin-2 (1–96) was purified on Mono Q column (GE Healthcare, Piscataway, NJ). Soluble unlabeled ternary SNARE complex comprise of syntaxin-1A (183–262), SNAP-25A (no cysteine), and synaptobrevin-2 (1–96). Syntaxin-1A (1–288)

monomer was labeled with Alexa Fluor 594 C5 maleimide at T197C. Protein structures were visualized with the program PyMOL (PDB ID: 1BYN for C2A, 1K5W for C2B, 1KIL for complexin, 3C98 for syntaxin-1A, and 1SFC, 3IPD for the SNARE complex)

Preparation of proteoliposomes

Lipid composition of liposomes (molar percentages) containing the Q-SNARE complex consists of 45% PC (L-α-phosphatidylcholine), 15% PE (L-α-phosphatidylethanolamine), 10% PS (L-α-phosphatidylserine), 25% Chol (cholesterol), 4% PI (L-α-phosphatidylinositol), and 1% PIP_2. In the case of increasing PIP_2 concentrations, PI contents were reduced accordingly. For FRET-based lipid-mixing assays, 3% PE was replaced with 1.5% 1,2-dioleoyl-sn-glycero-3-phosphoethanolamine-N-(7-nitrobenz-2-oxa-1,3-diazol-4-yl (NBD-DOPE) and 1.5% 1,2-dioleoyl-sn-glycero-3-phosphoethanolamine-N-lissamine rhodamine B sulfonyl ammonium salt (Rhodamine-DOPE) as a donor and an acceptor dye, respectively. Incorporation of the Q-SNARE complex into large unilamellar vesicles (LUVs) was achieved by OG (n-octyl-β-D-glucoside)-mediated reconstitution with protein-to-lipid molar ratio of 1:500, as described before[25].

Lipid-mixing assay

CG fusion *in vitro* was monitored using a lipid-mixing assay at 37 °C in 1 ml of buffer containing 120 mM K-glutamate, 20 mM K-acetate, 20 mM HEPES-KOH (pH 7.4), and 3 mM 2Na-ATP. $MgCl_2$ was added as indicated in the legends. 50 μg CGs and proteoliposomes containing NBD-DOPE and Rhodamine-DOPE as a donor and an acceptor dye, respectively, were incubated and lipid mixing led to dequenching of donor fluorescence (NBD) as a result of lipid dilution with unlabeled vesicle membrane[25,63]. Free Ca^{2+} concentrations in the presence of ATP and Mg^{2+} were calibrated using the Maxchelator simulation program (http://maxchelator.stanford.edu). Dequenching of the donor fluorescence (NBD) was measured using a Fluoromax spectrofluorometer (Horiba Jobin Yvon) using the wavelengths of 460 nm for excitation and 538 nm for emission, respectively. Dequenching of the donor fluorescence was normalized as the percentage value of the maximum donor fluorescence induced by 0.1% Triton X-100 detergent treatment at the end of fusion reactions.

Fluorescence anisotropy measurements

Wild-type and KAKA mutant versions of the C2AB fragment (20 nM, S342C) were labeled with Alexa Fluor 488[31]. Anisotropy measurements were carried out in a Fluorolog 3 spectrometer (Model FL322, Jobin Yvon) at 37 °C in 1 ml of buffer containing 120 mM K-glutamate, 20 mM K-acetate, and 20 mM HEPES-KOH (pH 7.4). $MgCl_2$ and ATP were added where indicated in the legends. Excitation wavelength was 495 nm and emission was measured at 520 nm. Lipid composition was identical to those used in a fusion assay except labeled PE (45% PC, 15% PE, 10% PS, 25% Chol, 4% PI, and 1% PIP_2).

Fluorescence resonance energy transfer (FRET)

Wild-type and KAKA mutant versions of C2AB (9 nM, S342C) were labeled with Alexa Fluor 488 as a donor dye. Alexa Fluor 647-labeled ATP or BODIPY TR-labeled ATP was used as an acceptor. Donor fluorescence was measured using Fluoromax (Horiba Jobin Yvon) using an excitation wavelength of 495 nm in 120 mM K-glutamate, 20 mM K-acetate, and 20 mM HEPES-KOH (pH 7.4). For binding experiments involving the SNARE complexes, SNAP-25A (Cys130) was labeled with Texas Red or syntaxin-1A (Cys197) was labeled with Alexa Fluor 594. Incubations were carried out in 20 mM HEPES-KOH (pH 7.4) containing either 50 mM or 150 mM KCl. Liposomes containing the SNARE proteins, i.e. in case of anionic phospholipids, were composed of 45% PC, 15% PE, 10% PS, 25% Chol, 4% PI, and 1% PIP_2, identical to those used in a fusion assay except labeled PE.

Isolation and culture of rat adrenal chromaffin cells

Animal care followed the University of Washington Animal Medicine guidelines. Adrenal glands were isolated from 5- to 8-week-old male Sprague Dawley rats euthanized by CO_2. Medullae were prepared by removing the cortex part of rat adrenal glands in ice cold Hank's balanced salt solution (HBSS) with 0.1% bovine serum albumin (BSA) and 10 mM HEPES. The medullae were cut into small pieces and incubated with 4 mg/mL collagenase type I (Sigma) for 25 min and 0.05% trypsin-EDTA (Invitrogen) for 20–30 min at 37°C to dissociate single chromaffin cells. The loose medulla tissue was triturated by gentle pipetting and suspended in culture medium (Dulbecco's Modified Eagle Medium (DMEM) containing 10% fetal bovine serum and 2% penicillin/streptomycin solution. The cell suspension was centrifuged at 1,200 rpm for 4 min at room temperature (22–25°C). The collected cells were resuspended in culture medium and plated on glass coverslips coated with poly-l-lysine. After 2 h, fresh culture medium was added, and the cells were maintained at 37°C in a 5% CO_2 incubator. Exocytosis was measured 1 – 2 days after cell preparation[64].

Dual-recording of Carbon fiber amperometry and whole-cell patch-clamping

Recordings of both carbon fiber amperometry and whole-cell patch-clamping were simultaneously performed on the same cell. Exocytosis was measured as pulses of electric current generated by oxidation of the molecules from single secretory vesicles at the tip of a carbon fiber electrode polarized to +400 mV. Carbon fiber microelectrodes were fabricated by using 11 μm carbon fibers and polypropylene 10 μl micropipette tips and backfilled with 3 M KCl[37]. The amperometric current signals were recorded with an EPC 9 patch-clamp amplifier with PatchMaster software (HEKA Elektronik), filtered at 0.1 kHz, and sampled digitally at 0.5 kHz.

Whole-cell patch configuration was achieved with an EPC 9 patch-clamp amplifier. Patch electrodes had a DC resistance between 3 and 5 MΩ when filled with internal solution. Bath solution (Ringer's) consisted of 137.5 mM NaCl, 2.5 mM KCl, 1 mM $MgCl_2$, 2 mM $CaCl_2$, 10 mM glucose, 10 mM HEPES (pH adjusted to 7.3 with NaOH). The pipette solutions contained the following (in mM): 50 μM free Ca^{2+} internal solution (free Ca^{2+} was estimated with Maxchelator simulation program), 105 K-glutamate, 15.7 $CaCl_2$, 15 EGTA, 1 $MgCl_2$, 5 Na_2-ATP, 0.3 Na_2-GTP, and 10 HEPES; 200 μM free Ca^{2+} internal solution, 105 K-glutamate, 17.16 $CaCl_2$, 15 EGTA, 1 $MgCl_2$, 5 Na_2-ATP, 0.3 Na_2-GTP, and 10

HEPES; 1 mM free Ca^{2+} internal solution, 100 K-glutamate, 19.43 $CaCl_2$, 15 EGTA, 1 $MgCl_2$, 5 Na_2-ATP, 0.3 Na_2-GTP, and 10 HEPES ; 4 mM free Ca^{2+} internal solution, 95 K-glutamate, 23.17 $CaCl_2$, 15 EGTA, 1 $MgCl_2$, 5 Na_2-ATP, 0.3 Na_2-GTP, and 10 HEPES; 15 mM free Ca^{2+} internal solution, 80 K-glutamate, 34.62 $CaCl_2$, 15 EGTA, 1 $MgCl_2$, 5 Na_2-ATP, 0.3 Na_2-GTP, and 10 HEPES. All pipette solutions were adjusted to pH 7.2 with KOH and calibrated free Ca^{2+} with a calcium-ion-selective electrode (Thermo. Electron Corporation, Beverly, MA, USA). A patch pipette was positioned on the opposite side of the cell from the carbon fiber.

Amperometric signals were recorded for 12 min after the formation of the whole-cell configuration with a holding potential of −60 mV and the recordings were semi-automatically analyzed by using software written in Igor (WaveMetrics, Lake Oswego, OR USA). The rate of exocytosis was defined as the number of amperometric spikes per min, and the average rate of exocytosis obtained during 3 min was determined between 5 and 8 min after formation of whole-cell configuration, i.e. start of perfusion of pipette solution into the cytoplasm. Experiments were performed at room temperature with a holding potential of −60 mV.

Stopped-flow spectroscopy

Kinetic experiments were carried out on an Applied Photophysics SX.20 stopped-flow spectrophotometer at 37 °C in 150 mM KCl, 20 mM HEPES, pH 7.4 with KOH, 1 mM $MgCl_2$, and 3 mM ATP plus 100 μM free Ca^{2+}. Different concentrations of C2AB labeled with Alexa Fluor 488 at S342C were mixed with equal volumes of Rhodamine-PE containing liposomes (consisting of 49% PC, 13% PE, 10% PS, 25% Chol, 1% PIP_2, and 2 % Rhodamine-DOPE) at 500 μM under pseudo-first order conditions. The excitation wavelength was set on 495 nm and a 590 nm cut-off filter was used to collect fluorescence emission of Rhodamine. The resulting time courses were fit to a single-exponential function:

$$F(t)=F_0+A_{obs}*e^{-k_{obs}*t}$$

where F(t) equals the observed fluorescence at time t, F_0 is the final fluorescence, A_{obs} equals the amplitude, and k_{obs} is the observed rate constant. Observed rate constants were plotted as a function of protein concentration and fitted with the equation:

$$k_{obs}=k_{on}[v]+k_{off}$$

where k_{on} represents the apparent association constant, and k_{off} the apparent dissociation rate constant.

EPR spectroscopy

Proteins (synaptotagmin and syntaxin) were spin labeled using a ten-fold excess of the sulfhydryl reactive spin label (1-oxyl-2,2,5,5,-tetramethylpyroline-3-methyl methanethiosulfonate) as described previously[7]. Double electron-electron resonance (DEER) was performed using a Bruker Elexsys E580 EPR spectrometer fitted with a stand-

alone Q-band bridge using an EN5107D2 dielectric resonator. Measurements were made on approximately 10–15 μL of sample that was loaded into quartz capillaries (2.0 mm ID × 2.4 mm OD) and flash frozen in a dry ice/isopropanol bath. DEER data were acquired using a 4-pulse sequence[65] with 16 and 32 ns π/2 and π observe pulses, respectively, and a 32 ns π pump pulse. The pump frequency was positioned to the maximum of the nitroxide spectrum and the observe frequency was offset 17–20 MHz lower than the pump frequency. The dipolar evolution data were processed and distance distributions determined using Tikhonov regularization incorporated in the DeerAnalysis2013 software package[60]. This program contains an error analysis routine that was used to assess the error introduced by subtraction of the intermolecular background form factor from the primary data.

Sites within the core SNARE complex and in C2AB where the spin-labeled side chain, R1 was attached. The core SNARE complex included SNAP-25A (full-length, no cysteine), syntaxin-1A (180–253) and synaptobrevin-2 (1–116)[66]. The distributions were calculated from a DFT based rotamer library[67] using the program MMM[68].

Liposome co-flotation assay

Small liposomes (small unilamellar vesicles, 40 nm in diameter, 80% PC and 20% PE) which contain the SNARE complex consisting of full-length syntaxin-1A (1–288), SNAP-25A, and soluble synaptobrevin-2 (aa 49–96) were incubated with the C2AB fragment of synaptotagmin-1 (97–421). Liposomes containing the SNARE complex float up to the buffer fraction through the gradient due to their buoyancy. C2AB which binds to the SNARE complex co-floats to the buoyant density together with liposomes, whereas free C2AB remains in the gradient. The samples (30 μl) were then mixed with sucrose (80 %, 30 μl) and a second sucrose layer (30 %, 40 μl) was gently applied followed by another layer of buffer (30 μl). The density gradient was centrifuged with a Beckman TL-100 ultracentrifuge (TLS55 rotor, 100 000 g, 4 °C, 30 min). 20 μl aliquots were carefully taken from the top of the gradient and analyzed by western blot using antibody against synaptotagmin-1 (Synaptic Systems, Göttingen, Germany; monoclonal antibodies 41.1).

Fluorescence cross-correlation spectroscopy (FCCS)

The tethering (docking) experiment was executed using FCCS as described earlier[47,69]. FCCS discriminates free or docked liposomes as liposomes pass through the focal volume (0.3 fL) of a dual colour confocal fluorescence microscope. Simultaneous dual detection of fluorescence bursts observed in the focal volume corresponds to docking of liposomes, the signals of which are then said to be cross-correlated. FCCS for tethering (docking) assay determines the tethering percentage between two particles labeled with different fluorescent dyes[47].

Mathematical model

For screening of negatively charged PIP_2 by divalent cations, the probabilities or fractions of the screened PIP_2 and of the free PIP_2 are described by the Poisson-Boltzmann-type[70,71]. The electric potential energy of a PIP_2 molecule depends on both the distance from and the valence of countercations. Upon screening, the mean distance between the screened PIP_2 and cation should be reduced and, accordingly, the electric potential energy ε_P of a screened

PIP_2 becomes lower than the energy ε_f of a free PIP_2. For simplicity, ε_f is taken to be zero ($\varepsilon_P < \varepsilon_f \equiv 0$) because what matters is just the energy difference between ε_P and ε_f. The fractions P_P and P_f of the screened PIP_2 and of the free PIP_2, respectively, are thus given by

$$P_P = \frac{C_X V_P e^{-\varepsilon_P/k_B T}}{e^{-\varepsilon_f/k_B T} + C_X V_P e^{-\varepsilon_P/k_B T}} = \frac{C_X V_P e^{-\varepsilon_P/k_B T}}{1 + C_X V_P e^{-\varepsilon_P/k_B T}}, \quad (1)$$

$$P_f = \frac{e^{-\varepsilon_f/k_B T}}{e^{-\varepsilon_f/k_B T} + C_X V_P e^{-\varepsilon_P/k_B T}} = \frac{1}{1 + C_X V_P e^{-\varepsilon_P/k_B T}}, \quad (2)$$

where V_P denotes the effective volume in which PIP_2 can encounter cations of concentration C_X, k_B the Boltzmann constant, and the absolute temperature. The cations that screen PIP_2 (X) are denoted as M and C for Mg^{2+} and Ca^{2+}, respectively; where and represent the concentrations of Mg^{2+} and Ca^{2+}. Note that the denominator, $1 + C_X V_P e^{-\varepsilon P/k_B T}$, is a normalization factor that ensures. $P_P + P_f = 1$.

Those fractions can be written in the form of a simple Hill-type equation which is widely used for biochemical reactions:[72] $P_P = C_X (C_0 + C_X)^{-1}$ and $P_f = C_0 (C_0 + C_X)^{-1}$ with $C_0 \equiv V_P^{-1} e^{\varepsilon_P/k_B T}$. The resulting fractions P_P and P_f depend on the cation concentration and are illustrated in Supplementary Fig. 7d. The result provides the range of cation concentrations that screen PIP_2. Millimolar concentrations of divalent cations turn out to be effective when we use the parameters obtained from fitting of the experimental data (Figs. 1d, 2c, and 2d) to the present model. The concentration of effective (free) PIP_2 then takes the form

$$C_P^{(e)} = C_P P_f = \frac{C_P}{1 + C_X V_P e^{-\varepsilon_P/k_B T}}, \quad (3)$$

where C_P represents the total concentration of PIP_2.

We next describe the bound fraction of C2AB domains saturated by free PIP_2, as a function of the free (effective) PIP_2 concentration $C_P^{(e)}$:

$$F_b = \frac{1}{1 + \frac{K_{PC}}{C_P^{(e)} C_C^{(e)}}}, \quad (4)$$

where K_{PC} is the dissociation constant of the PIP_2-C2AB coordination and $C_P^{(e)}$ the effective Ca^{2+} concentration. We assume that $K_{PC} \equiv \frac{[\mathrm{C2AB}][\mathrm{Ca}^{2+}][\mathrm{PIP_2}]}{[\mathrm{C2AB} - \mathrm{Ca}^{2+} - \mathrm{PIP_2}]}$ for the trans-binding is given by the product of the dissociation constants $K_C \equiv \frac{[\mathrm{C2AB}][\mathrm{Ca}^{2+}]}{[\mathrm{C2AB} - \mathrm{Ca}^{2+}]}$ and $K_P \equiv \frac{[\mathrm{C2AB} - \mathrm{Ca}^{2+}][\mathrm{PIP_2}]}{[\mathrm{C2AB} - \mathrm{Ca}^{2+} - \mathrm{PIP_2}]}$ of the C2AB-Ca^{2+} binding and of the Ca^{2+}-mediated C2AB-PIP_2 binding, respectively.

By combining Eqs. (3) and (4), the fraction of PIP_2-bound C2AB can be described as a function of the cation concentration C_X ($X = M$ or C):

$$F_b(C_X)=\frac{C_C^{(e)}C_P}{C_C^{(e)}C_P+K_{PC}(1+C_X V_P e^{-\varepsilon_P/k_B T})}. \quad (5)$$

Now we can determine the nonlinear behavior of trans-binding of C2AB to PIP_2 at different Ca^{2+} concentrations (Fig. 2c). For simplicity, fluorescence anisotropy y is assumed to be proportional to bound fraction F_b of C2AB domains, i.e. $y = a_C F_b$ with an appropriate constant a_C. This relation, together with Eq. (5) for $C_X = C_C$ allows us to fit the experimental data (Fig. 2c):

$$y=a_C F_b(C_C)=\frac{a_C C_C^{(e)}C_P}{C_C^{(e)}C_P+K_{PC}(1+C_C V_P e^{-\varepsilon_P/k_B T})}, \quad (6)$$

where the coordination effects of Ca^{2+} have been taken into account by the effective Ca^{2+} concentration acting on the trans-binding, $C_C^{(e)}=\kappa {C_C}^n(\lambda^n+{C_C}^n)^{-1} \equiv C_{C,\kappa}^{(e)}$ with the maximum effective Ca^{2+} concentration κ, displaying saturation due to the limited numbers of coordination counter parts. Here λ measures the characteristic Ca^{2+} concentration at which the effective concentration reaches half the maximum, i.e., $C_C^{(e)}(C_C=\lambda)=\kappa/2$, and the exponent n of Ca^{2+} cooperativity is determined from the biological experiment in Ref.[73]. The fitting of our experimental data with Eq. (6) is quite satisfactory for both the increase of PIP_2-C2AB complex as mediated by Ca^{2+} and its decrease due to PIP_2 screening by Ca^{2+}. The parameters obtained from the fitting are listed in Supplementary Table 1.

Furthermore, the PIP_2 screening model successfully describes PIP_2-C2AB trans-binding (Fig. 1d) at different Mg^{2+} concentrations. For this fitting we have used the parameters in Table 1.

The model has also been extended to the system of PS-mediated cis-binding (Fig. 2d). Similarly to PIP_2-mediated trans-binding, C2AB binding (% max) in the PS-mediated cis-binding, is given by a function of C_C with an appropriate constant c_C:

$$y=c_C F_b(C_C)=\frac{c_C C_C^{(e)}C_S}{C_C^{(e)}C_S+K_{SC}(1+C_C V_S e^{-\varepsilon_S/k_B T})}, \quad (9)$$

where $C_S$denotes the total concentration of PS, K_{SC} the equilibrium dissociation constant for cis-binding, V_S the effective volume of PS, and ε_S the electric potential energy of a screened PS. Again, in consideration of the limited numbers of PS and C2AB domains, we have the effective Ca^{2+} concentration acting on the cis-binding: $C_C^{(e)}=C_{C,\mu}^{(e)} \equiv \mu {C_C}^n(\nu^n+{C_C}^n)^{-1}$ with the maximum (saturation) concentration μ and the characteristic Ca^{2+} concentration corresponding to half the maximum effective concentration. Equation (9) could fit the non-monotonic behavior of the cis-binding between PS and C2AB domains (line in Fig. 2d).

Statistical analysis

The statistical difference between two groups was evaluated by Student's t-test. Probabilities of $P \leq 0.05$ (*) were considered significant.

Supplementary Material

Refer to Web version on PubMed Central for supplementary material.

Acknowledgements

We appreciate Dr. Bertil Hille for helpful discussion. This research was supported by US National Institutes of Health Grant (DK080840 to D.S.K.), National Research Foundation of Korea through the Basic Science Research Program (2012R1A2A4A01004419 and 2011-0012331 to M.Y.C), and US National Institutes of Health (2 P01 GM072694 to R.J. and D.S.C.).

References

1. Sudhof TC. Neurotransmitter release: the last millisecond in the life of a synaptic vesicle. Neuron. 2013; 80:675–690. [PubMed: 24183019]
2. Jahn R, Fasshauer D. Molecular machines governing exocytosis of synaptic vesicles. Nature. 2012; 490:201–207. [PubMed: 23060190]
3. Pobbati AV, Stein A, Fasshauer D. N- to C-terminal SNARE complex assembly promotes rapid membrane fusion. Science. 2006; 313:673–676. [PubMed: 16888141]
4. Perin MS, Fried VA, Mignery GA, Jahn R, Sudhof TC. Phospholipid binding by a synaptic vesicle protein homologous to the regulatory region of protein kinase C. Nature. 1990; 345:260–263. [PubMed: 2333096]
5. Brose N, Petrenko AG, Sudhof TC, Jahn R. Synaptotagmin: a calcium sensor on the synaptic vesicle surface. Science. 1992; 256:1021–1025. [PubMed: 1589771]
6. Davletov BA, Sudhof TC. A single C2 domain from synaptotagmin I is sufficient for high affinity Ca2+/phospholipid binding. J Biol Chem. 1993; 268:26386–26390. [PubMed: 8253763]
7. Herrick DZ, Sterbling S, Rasch KA, Hinderliter A, Cafiso DS. Position of synaptotagmin I at the membrane interface: cooperative interactions of tandem C2 domains. Biochemistry. 2006; 45:9668–9674. [PubMed: 16893168]
8. Fernandez I, et al. Three-dimensional structure of the synaptotagmin 1 C2B–domain: synaptotagmin 1 as a phospholipid binding machine. Neuron. 2001; 32:1057–1069. [PubMed: 11754837]
9. Arac D, et al. Close membrane-membrane proximity induced by Ca(2+)-dependent multivalent binding of synaptotagmin-1 to phospholipids. Nat Struct Mol Biol. 2006; 13:209–217. [PubMed: 16491093]
10. Wang Z, Liu H, Gu Y, Chapman ER. Reconstituted synaptotagmin I mediates vesicle docking, priming, and fusion. J Cell Biol. 195:1159–1170. [PubMed: 22184197]
11. Honigmann A, et al. Phosphatidylinositol 4,5-bisphosphate clusters act as molecular beacons for vesicle recruitment. Nat Struct Mol Biol. 2013; 20:679–686. [PubMed: 23665582]
12. van den Bogaart G, et al. Membrane protein sequestering by ionic protein-lipid interactions. Nature. 2011; 479:552–555. [PubMed: 22020284]
13. Suh BC. Hille, BPIP2 is a necessary cofactor for ion channel function: how and why? Annu Rev Biophys. 2008; 37:175–195. [PubMed: 18573078]
14. Tucker SJ, Baukrowitz T. How highly charged anionic lipids bind and regulate ion channels. J Gen Physiol. 2008; 131:431–438. [PubMed: 18411329]
15. McLaughlin S, Murray D. Plasma membrane phosphoinositide organization by protein electrostatics. Nature. 2005; 438:605–611. [PubMed: 16319880]
16. Helmholtz H. Ueber einige Gesetze der Vertheilung elektrischer Ströme in körperlichen Leitern mit Anwendung auf die thierischelektrischen Versuche. Pogg Ann. 1853; 89

17. Manning GS, Ray J. Counterion condensation revisited. J Biomol Struct Dyn. 1998; 16:461–476. [PubMed: 9833682]
18. Delgado AV, et al. Measurement and interpretation of electrokinetic phenomena. J Colloid Interface Sci. 2007; 309:194–224. [PubMed: 17368660]
19. Schiavo G, Stenbeck G, Rothman JE, Sollner TH. Binding of the synaptic vesicle v-SNARE, synaptotagmin, to the plasma membrane t-SNARE, SNAP-25, can explain docked vesicles at neurotoxin-treated synapses. Proc Natl Acad Sci U S A. 1997; 94:997–1001. [PubMed: 9023371]
20. Rickman C, Davletov B. Mechanism of calcium-independent synaptotagmin binding to target SNAREs. J Biol Chem. 2003; 278:5501–5504. [PubMed: 12496268]
21. Rickman C, et al. Conserved prefusion protein assembly in regulated exocytosis. Mol Biol Cell. 2006; 17:283–294. [PubMed: 16267273]
22. Chicka MC, Hui E, Liu H, Chapman ER. Synaptotagmin arrests the SNARE complex before triggering fast, efficient membrane fusion in response to Ca2+ Nat Struct Mol Biol. 2008; 15:827–835. [PubMed: 18622390]
23. Brewer KD, et al. Dynamic binding mode of a Synaptotagmin-1-SNARE complex in solution. Nat Struct Mol Biol. 2015
24. Li L, et al. Phosphatidylinositol phosphates as co-activators of Ca2+ binding to C2 domains of synaptotagmin 1. J Biol Chem. 2006; 281:15845–15852. [PubMed: 16595652]
25. Park Y, et al. Controlling synaptotagmin activity by electrostatic screening. Nat Struct Mol Biol. 19:991–997. [PubMed: 22940675]
26. Chapman ER. How does synaptotagmin trigger neurotransmitter release? Annu Rev Biochem. 2008; 77:615–641. [PubMed: 18275379]
27. Rizo J, Rosenmund C. Synaptic vesicle fusion. Nat Struct Mol Biol. 2008; 15:665–674. [PubMed: 18618940]
28. Choi UB, et al. Single-molecule FRET-derived model of the synaptotagmin 1-SNARE fusion complex. Nat Struct Mol Biol. 2010; 17:318–324. [PubMed: 20173763]
29. Tang J, et al. A complexin/synaptotagmin 1 switch controls fast synaptic vesicle exocytosis. Cell. 2006; 126:1175–1187. [PubMed: 16990140]
30. Bai J, Tucker WC, Chapman ER. PIP2 increases the speed of response of synaptotagmin and steers its membrane-penetration activity toward the plasma membrane. Nat Struct Mol Biol. 2004; 11:36–44. [PubMed: 14718921]
31. Radhakrishnan A, Stein A, Jahn R, Fasshauer D. The Ca2+ affinity of synaptotagmin 1 is markedly increased by a specific interaction of its C2B domain with phosphatidylinositol 4,5-bisphosphate. J Biol Chem. 2009; 284:25749–25760. [PubMed: 19632983]
32. Lee HK, et al. Dynamic Ca2+-dependent stimulation of vesicle fusion by membrane-anchored synaptotagmin 1. Science. 2010; 328:760–763. [PubMed: 20448186]
33. Toner M, Vaio G, McLaughlin A, McLaughlin S. Adsorption of cations to phosphatidylinositol 4,5-bisphosphate. Biochemistry. 1988; 27:7435–7443. [PubMed: 2849993]
34. Suh BC, Hille B. Electrostatic interaction of internal Mg2+ with membrane PIP2 Seen with KCNQ K+ channels. J Gen Physiol. 2007; 130:241–256. [PubMed: 17724161]
35. Knight DE, Baker PF. Calcium-dependence of catecholamine release from bovine adrenal medullary cells after exposure to intense electric fields. J Membr Biol. 1982; 68:107–140. [PubMed: 6809949]
36. Wegenhorst U, Gratzl M, Fohr KJ, Ahnert-Hilger G. Millimolar concentrations of free magnesium enhance exocytosis from permeabilized rat pheochromocytoma (PC 12) cells. Neurosci Lett. 1989; 106:300–304. [PubMed: 2601884]
37. Koh DS. Carbon fiber amperometry in the study of ion channels and secretion. Methods Mol Biol. 2006; 337:139–153. [PubMed: 16929945]
38. Kuo W, Herrick DZ, Ellena JF, Cafiso DS. The calcium-dependent and calcium-independent membrane binding of synaptotagmin 1: two modes of C2B binding. J Mol Biol. 2009; 387:284–294. [PubMed: 19302798]
39. Vrljic M, et al. Post-translational modifications and lipid binding profile of insect cell-expressed full-length mammalian synaptotagmin 1. Biochemistry. 50:9998–10012. [PubMed: 21928778]

40. Jeschke G, Koch A, Jonas U, Godt A. Direct conversion of EPR dipolar time evolution data to distance distributions. Journal of magnetic resonance. 2002; 155:72–82. [PubMed: 11945035]
41. Pannier M, Veit S, Godt A, Jeschke G, Spiess HW. Dead-Time Free Measurement of Dipole-Dipole Interactions between Electron Spins. Journal of Magnetic Resonance. 2000; 142:331–340. [PubMed: 10648151]
42. Beis I, Newsholme EA. The contents of adenine nucleotides, phosphagens and some glycolytic intermediates in resting muscles from vertebrates and invertebrates. Biochem J. 1975; 152:23–32. [PubMed: 1212224]
43. London RE. Methods for measurement of intracellular magnesium: NMR and fluorescence. Annu Rev Physiol. 1991; 53:241–258. [PubMed: 2042961]
44. Hess P, Metzger P, Weingart R. Free magnesium in sheep, ferret and frog striated muscle at rest measured with ion-selective micro-electrodes. J Physiol. 1982; 333:173–188. [PubMed: 6820662]
45. Rickman C, et al. Synaptotagmin interaction with the syntaxin/SNAP-25 dimer is mediated by an evolutionarily conserved motif and is sensitive to inositol hexakisphosphate. J Biol Chem. 2004; 279:12574–12579. [PubMed: 14709554]
46. Gaffaney JD, Dunning FM, Wang Z, Hui E, Chapman ER. Synaptotagmin C2B domain regulates Ca2+-triggered fusion in vitro: critical residues revealed by scanning alanine mutagenesis. J Biol Chem. 2008; 283:31763–31775. [PubMed: 18784080]
47. Vennekate W, et al. Cis- and trans-membrane interactions of synaptotagmin-1. Proc Natl Acad Sci U S A. 2012; 109:11037–11042. [PubMed: 22711810]
48. Shao X, et al. Synaptotagmin-syntaxin interaction: the C2 domain as a Ca2+-dependent electrostatic switch. Neuron. 1997; 18:133–142. [PubMed: 9010211]
49. Sarhan S, Seiler N. On the subcellular localization of the polyamines. Biol Chem Hoppe Seyler. 1989; 370:1279–1284. [PubMed: 2482746]
50. Dai H, Shen N, Arac D, Rizo J. A quaternary SNARE-synaptotagmin-Ca2+-phospholipid complex in neurotransmitter release. J Mol Biol. 2007; 367:848–863. [PubMed: 17320903]
51. Lynch KL, et al. Synaptotagmin C2A loop 2 mediates Ca2+-dependent SNARE interactions essential for Ca2+-triggered vesicle exocytosis. Mol Biol Cell. 2007; 18:4957–4968. [PubMed: 17914059]
52. Lai AL, Huang H, Herrick DZ, Epp N, Cafiso DS. Synaptotagmin 1 and SNAREs form a complex that is structurally heterogeneous. J Mol Biol. 2011; 405:696–706. [PubMed: 21087613]
53. Lai Y, Lou X, Diao J, Shin YK. Molecular origins of synaptotagmin 1 activities on vesicle docking and fusion pore opening. Sci Rep. 2015; 5:9267. [PubMed: 25791821]
54. Lai AL, Tamm LK, Ellena JF, Cafiso DS. Synaptotagmin 1 modulates lipid acyl chain order in lipid bilayers by demixing phosphatidylserine. J Biol Chem. 2011; 286:25291–25300. [PubMed: 21610074]
55. Martens S, Kozlov MM, McMahon HT. How synaptotagmin promotes membrane fusion. Science. 2007; 316:1205–1208. [PubMed: 17478680]
56. Hui E, Johnson CP, Yao J, Dunning FM, Chapman ER. Synaptotagmin-mediated bending of the target membrane is a critical step in Ca(2+)-regulated fusion. Cell. 2009; 138:709–721. [PubMed: 19703397]
57. McMahon HT, Kozlov MM, Martens S. Membrane curvature in synaptic vesicle fusion and beyond. Cell. 2010; 140:601–605. [PubMed: 20211126]
58. van den Bogaart G, et al. Synaptotagmin-1 may be a distance regulator acting upstream of SNARE nucleation. Nat Struct Mol Biol. 2011; 18:805–812. [PubMed: 21642968]
59. Imig C, et al. The morphological and molecular nature of synaptic vesicle priming at presynaptic active zones. Neuron. 2014; 84:416–431. [PubMed: 25374362]
60. Jeschke G, et al. DeerAnalysis2006—a comprehensive software package for analyzing pulsed ELDOR data. Applied Magnetic Resonance. 2006; 30:473–498.

References for Online Methods

60. Weber T, et al. SNAREpins: minimal machinery for membrane fusion. Cell. 1998; 92:759–772. [PubMed: 9529252]
61. Stein A, Radhakrishnan A, Riedel D, Fasshauer D, Jahn R. Synaptotagmin activates membrane fusion through a Ca2+-dependent trans interaction with phospholipids. Nat Struct Mol Biol. 2007; 14:904–911. [PubMed: 17891149]
62. Park Y, et al. alpha-SNAP interferes with the zippering of the SNARE protein membrane fusion machinery. J Biol Chem. 2014; 289:16326–16335. [PubMed: 24778182]
63. Zhou Z, Misler S. Action potential-induced quantal secretion of catecholamines from rat adrenal chromaffin cells. J Biol Chem. 1995; 270:3498–3505. [PubMed: 7876083]
64. Pannier M, Veit S, Godt A, Jeschke G, Spiess HW. Dead-time free measurement of dipole-dipole interactions between electron spins. J Magn Reson. 2000; 142:331–340. [PubMed: 10648151]
65. Stein A, Weber G, Wahl MC, Jahn R. Helical extension of the neuronal SNARE complex into the membrane. Nature. 2009; 460:525–528. [PubMed: 19571812]
66. Warshaviak DT, Serbulea L, Houk KN, Hubbell WL. Conformational analysis of a nitroxide side chain in an alpha-helix with density functional theory. J Phys Chem B. 2011; 115:397–405. [PubMed: 21162593]
67. Polyhach Y, Bordignon E, Jeschke G. Rotamer libraries of spin labelled cysteines for protein studies. Phys Chem Chem Phys. 2011; 13:2356–2366. [PubMed: 21116569]
68. Cypionka A, et al. Discrimination between docking and fusion of liposomes reconstituted with neuronal SNARE-proteins using FCS. Proc Natl Acad Sci U S A. 2009; 106:18575–18580. [PubMed: 19843696]
69. Fogolari F, Brigo A, Molinari H. The Poisson-Boltzmann equation for biomolecular electrostatics: a tool for structural biology. J Mol Recognit. 2002; 15:377–392. [PubMed: 12501158]
70. Li C, Li L, Petukh M, Alexov E. Progress in developing Poisson-Boltzmann equation solvers. Mol Based Math Biol. 2013; 1
71. Hill AV. The Combinations of Haemoglobin with Oxygen and with Carbon Monoxide. I. Biochem J. 1913; 7:471–480. [PubMed: 16742267]
72. Augustine GJ, Neher E. Calcium requirements for secretion in bovine chromaffin cells. J Physiol. 1992; 450:247–271. [PubMed: 1432709]

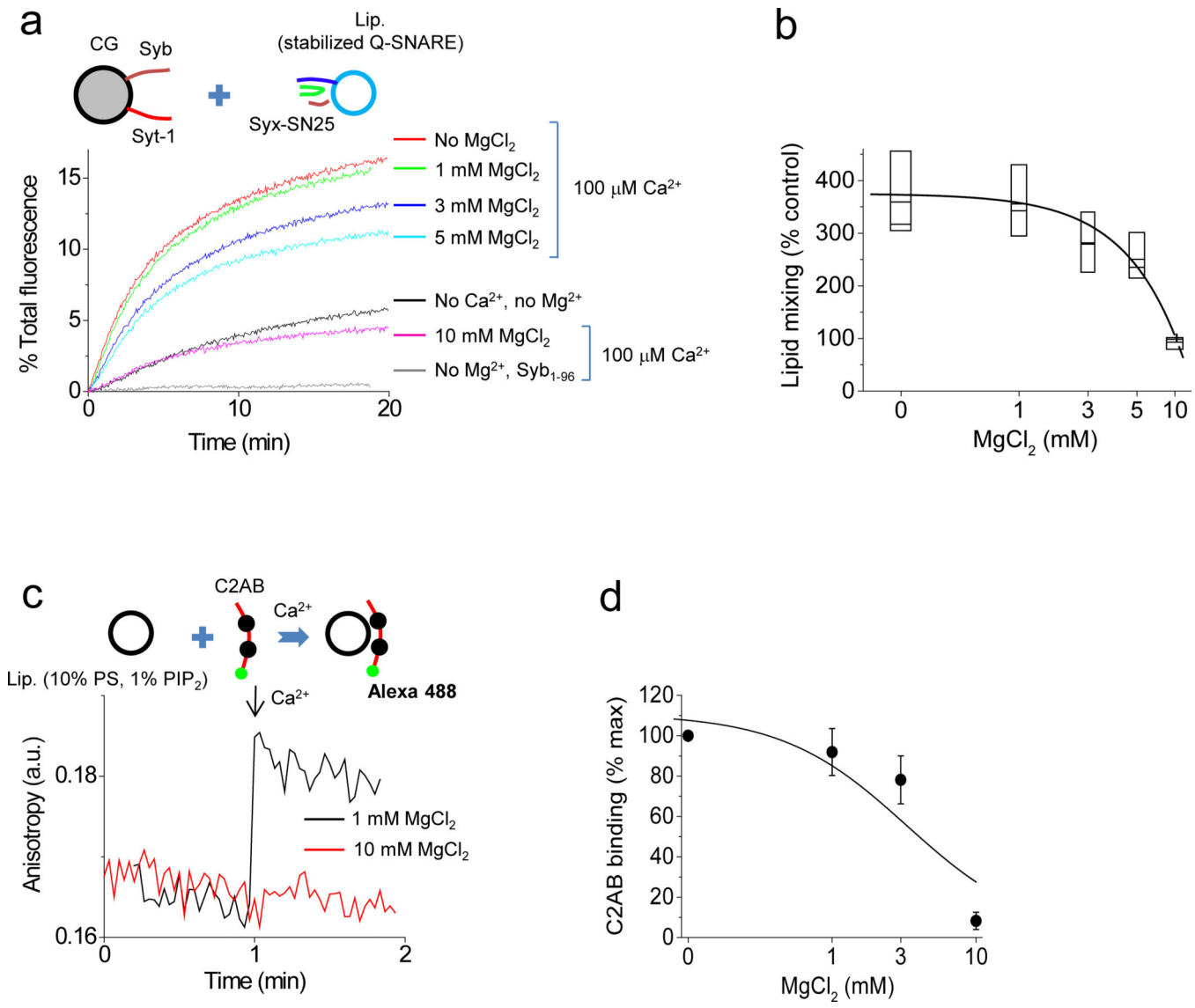

Figure 1. High concentrations of Mg^{2+} ions inhibit Ca^{2+}-dependent and synaptotagmin-1-mediated fusion

(**a**) Lipid-mixing between purified chromaffin granules (CGs) and liposomes containing a stabilized Q-SNARE complex (Syx-SN25)[3] (see Online Methods for details). The liposomes contained a standard mixture of membrane lipids including 10% phosphatidylserine (PS), 1% PIP_2, 1.5% NBD-PE, and 1.5% Rhodamine-PE. CG fusion is given as percentage of maximum donor fluorescence (total fluorescence) after addition of 0.1% Triton X-100. (**b**) Dose-response curve of $MgCl_2$ on Ca^{2+}-dependent CG fusion obtained from (**a**). Lipid mixing at 5 min after fusion reaction was quantified as percentage by normalizing to control, basal fusion without any treatment of Mg^{2+} or Ca^{2+} (n=3, range of values is indicated, lines within the boxes represent individual data points). (**c,d**) Binding of the C2AB fragment of synaptotagmin-1 ($Syt_{97–421}$)[31] to protein-free liposomes, measured by fluorescence anisotropy (Lip., lipid composition as in (**a**) except that the labelled lipids were omitted). Binding was triggered by adding 100 μM free Ca^{2+} at different concentrations of $MgCl_2$.

a.u., arbitrary units. (**d**) Dose-response curve of $MgCl_2$ on Ca^{2+}-dependent C2AB binding. C2AB binding is plotted as percentage of maximum value induced by 100 μM Ca^{2+} in the absence of Mg^{2+}. Data for **d** are mean ± SD from four independent experiments. The line in **d** shows the fit of experimental data with our mathematical model (see Online Methods for details). Normal ionic strength, i.e. 140 mM K^+ and 3 mM ATP for anisotropy and fusion assay.

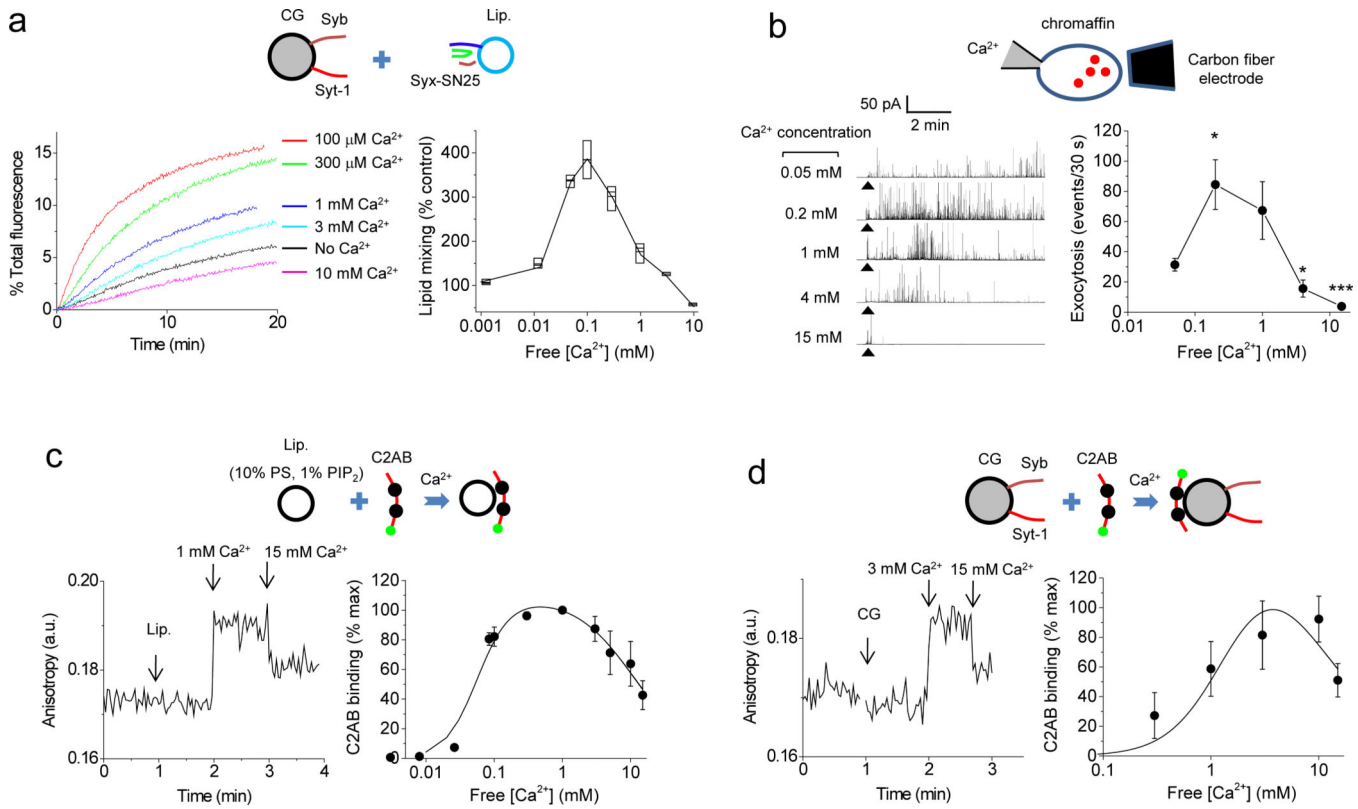

Figure 2. Biphasic effect of Ca^{2+} on CG fusion *in vitro* and in intact cells

(**a**) Left: Lipid-mixing between CGs and SNARE-containing liposomes as described in Fig. 1a at different concentrations of Ca^{2+} in the presence of 1 mM $MgCl_2$. Right: Dose-response curve of a lipid-mixing assay at various Ca^{2+} concentrations. The degree of fusion at 5 min after start of the reaction is normalized to fusion in the absence of Ca^{2+} (control) that was set to 100% (n=3, range of values is indicated). (**b**) Left: Exocytotic events of rat chromaffin cells recorded by carbon fiber amperometry. The arrowhead indicates the formation of whole-cell patch clamping (W-C) configuration at 30 s. Right: The rate of exocytosis was calculated as number of amperometric events per 30 s (events/30 s). Average values from 5–17 independent experiments. Data are means ± SEM. * $P < 0.05$ and *** $P < 0.001$ compared to the exocytosis triggered by 50 μM Ca^{2+}. (**c,d**) Ca^{2+} dose-response curve for synaptotagmin-1 (C2AB) binding to liposomes (**c**, 10% PS and 1% PIP_2) and purified CGs (**d**). 1 mM $MgCl_2$ was included as in the fusion assay as in (**a**). C2AB binding to liposomes or CG membranes is presented as percentage of maximum value. Anisotropy data from **c** and **d** were fitted with the mathematical model. 140 mM K^+ and 3 mM ATP for anisotropy and fusion assay. Data for **c,d** are mean ± SD from four independent experiments.

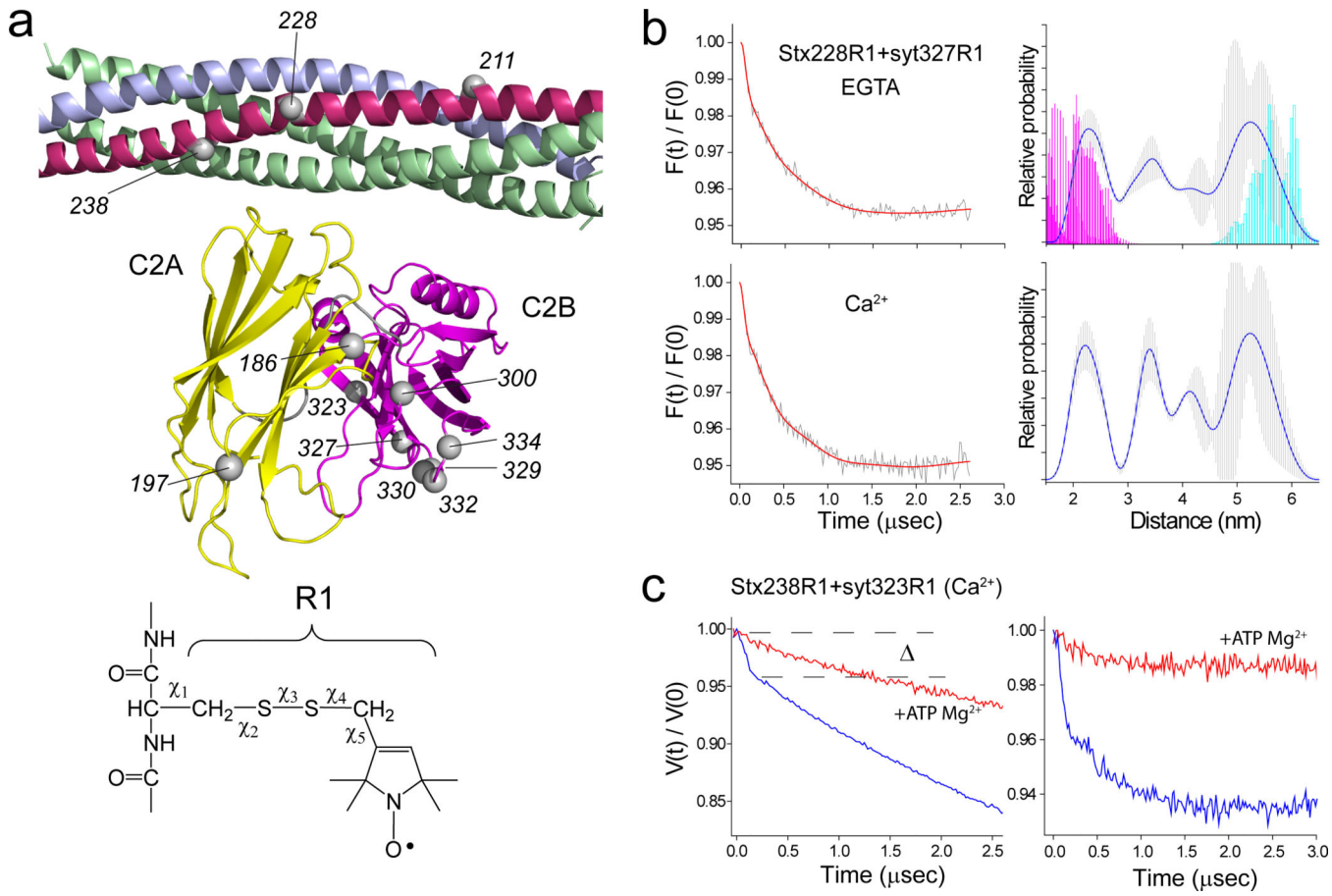

Figure 3. Heterogeneous interaction of synaptotagmin-1-SNARE complex

(**a**) The α-carbons of the spin-labeled side chain are shown in grey, syntaxin-1A is in red, synaptobrevin-2 in blue, SNAP-25A in green, synaptotagmin-1 (syt1) C2A in yellow, and C2B in magenta. (**b**) Background subtracted DEER data (grey traces, left panels) obtained for a mixture of 50 μM syt1 327R1 and 50 μM core SNARE complex labeled at site 228 in the H3 segment of syntaxin-1A (Stx). Data in the upper and lower panels were obtained either in the presence of EGTA or 1 mM Ca^{2+}, respectively. The left panels also show the best fit in the time domain to the data using the model free fit in DeerAnalysis (red trace)[60]. The panels on the right show the distance distributions corresponding to the best fit (blue trace). The error bars in the distribution (grey shading) represent uncertainty in the subtraction of the intermolecular signal that produces fits within 15% RMSD of the best fit. The cyan and magenta histograms represent the predicted distances based upon the model generated from smFRET data[28] and the the five MD models[23], respectively. (**c**) Raw DEER data (left panel) and background subtracted DEER signals (right panel) obtained for the Stx 238R1/syt1 323 R1 spin pair in the absence (blue trace) and presence (red trace) of 2 mM Mg^{2+}/ATP. In the left panel, the modulation depth, Δ, represents the fraction of the signal that results from an intramolecular dipole-dipole interaction.

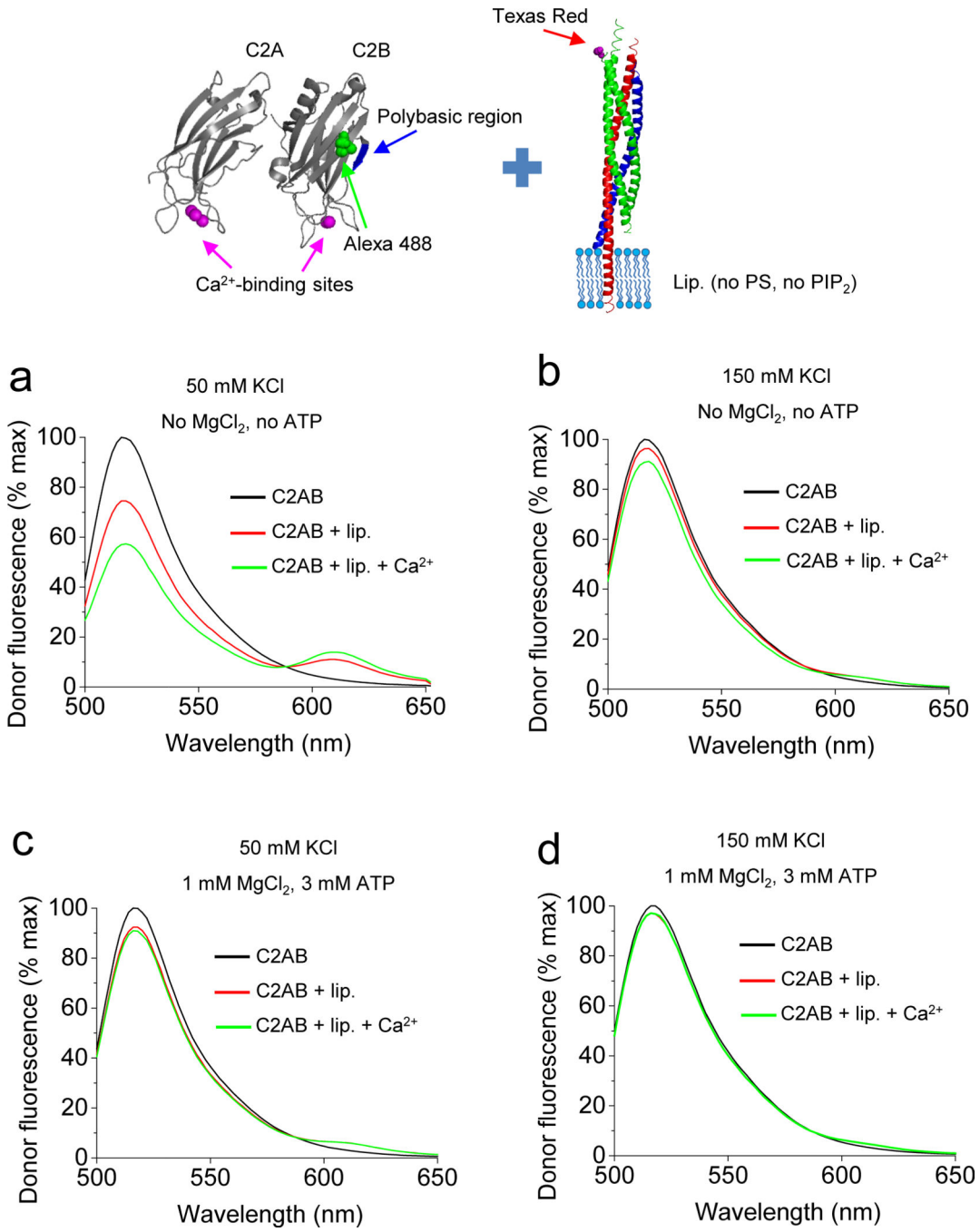

Figure 4. Mg^{2+} and ATP eliminate binding of synaptotagmin-1 to SNARE complexes reconstituted in liposomes free of acidic lipids

Binding of synaptotagmin-1 to the SNARE complexes reconstituted in liposomes (Lip.) devoid of acidic phospholipids, measured by FRET. A preformed ternary SNARE complex containing synaptobrevin-2 (1–96, blue), SNAP-25A (green) labeled with Texas Red indicated by an arrow at position 130C (single cysteine mutant), and syntaxin-1A (183–288, red) was reconstituted in liposomes containing 80% PC and 20% PE. The C2AB fragment of synaptotagmin-1 was labeled with Alexa Fluor 488 at 342C (indicated by green dots). The polybasic region is shown in blue and Ca^{2+} in magenta. Donor emission fluorescence

spectra of Alexa Fluor 488 were recorded for C2AB in the indicated buffers, either alone (black), or in the presence of SNARE-liposomes (red) or in the presence of SNARE liposomes and 1 mM Ca^{2+}. (**a**) 50 mM KCl, no Mg^{2+}/ATP, (b) 150 mM KCl, no Mg^{2+}/ATP, (c) 50 mM KCl plus Mg^{2+}/ATP, (d) 150 mM KCl, plus Mg^{2+}/ATP,. Donor fluorescence was normalized as percentage of maximum value. Shown are representative donor emission fluorescence spectra from 3 to 5 independent experiments.

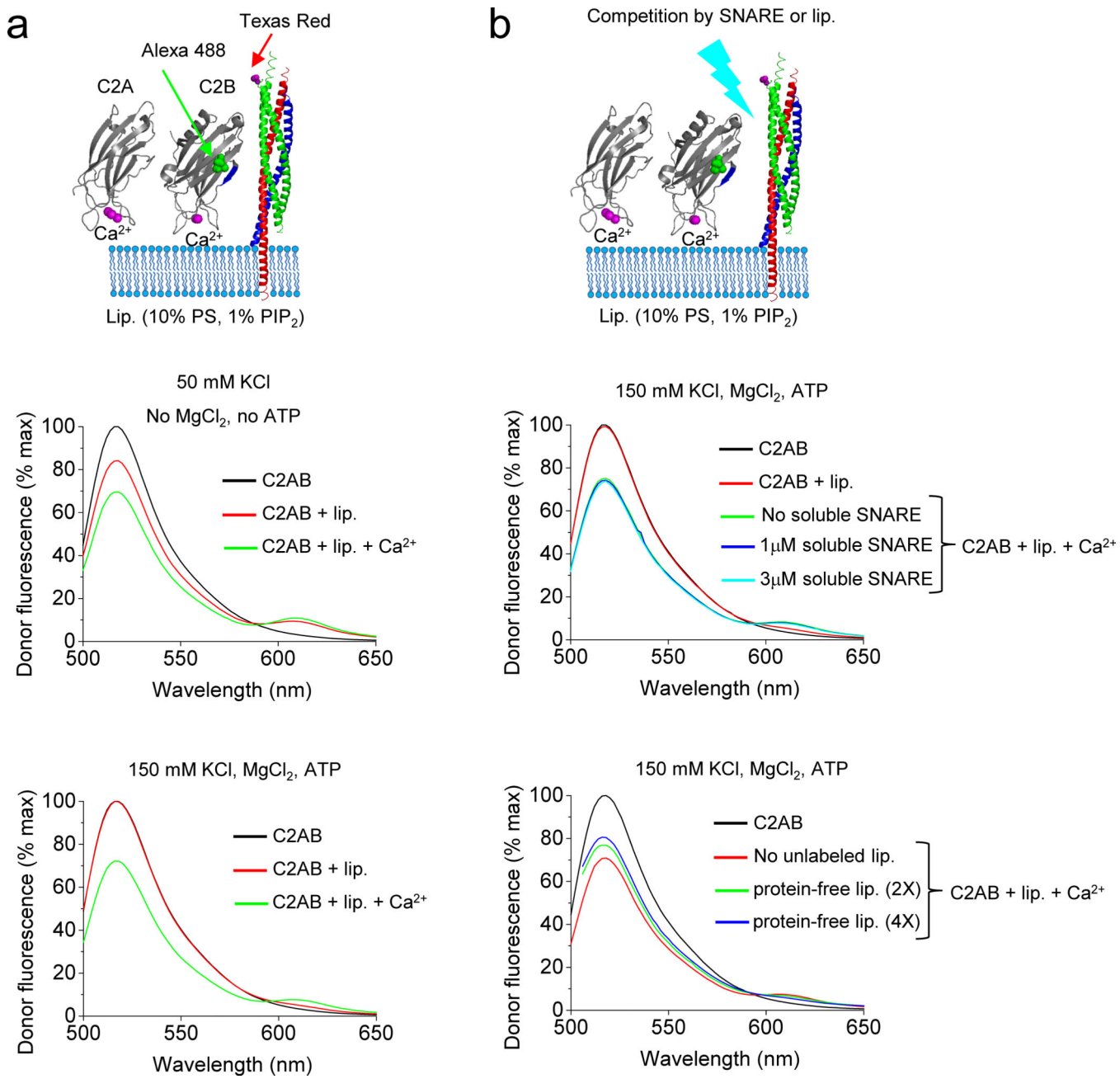

Figure 5. Mg^{2+} and ATP eliminate binding of synaptotagmin-1 to SNARE complexes reconstituted in liposomes containing acidic lipids and PIP_2

(**a**) Donor emission fluorescence spectra for binding of the C2AB fragment to the reconstituted SNARE complex as described in Fig. 4. Liposomes contained 10% PS and 1% PIP_2 as in Fig. 1c,2c (see Online Methods for details). Binding was monitored either at 50 mM KCl in the absence of Mg^{2+}/ATP (**a,middle**) or at 150 mM KCl in the presence of 1 mM $MgCl_2$ and 3 mM ATP (**a,bottom**). (**b**) Effect of excess unlabeled soluble SNARE complexes (**b, middle**) and excess protein-free liposomes (**b, bottom**). All donor emission fluorescence spectra with an excitation wavelength are representative from 3 to 5 independent experiments.

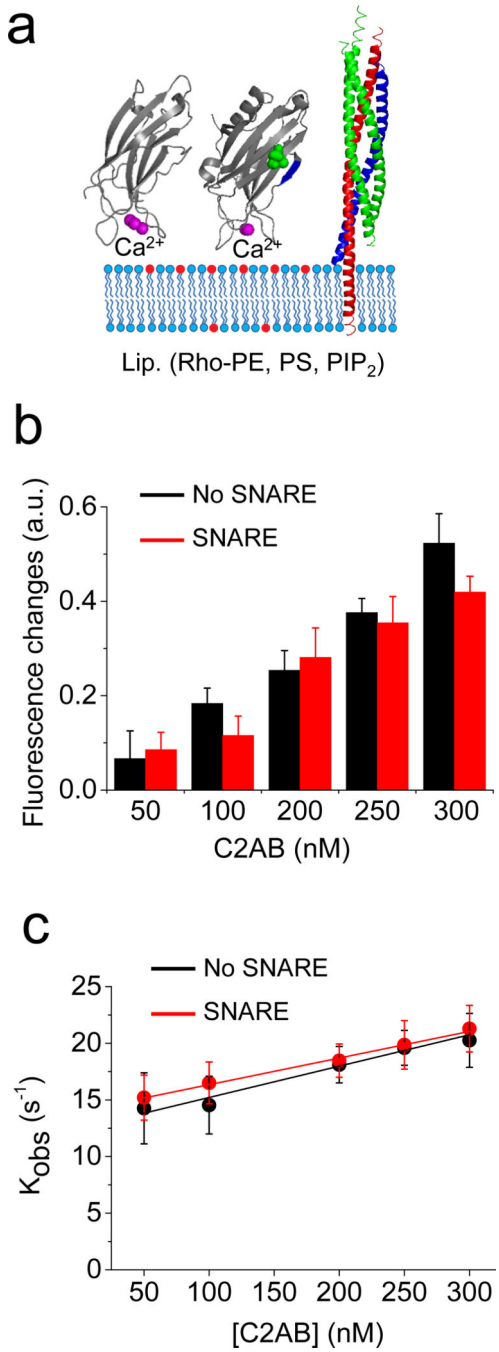

Figure 6. Synaptotagmin-1 binds to membranes containing PIP_2 but not to membranes containing SNARE complexes

(**a–c**) Stopped-flow spectroscopy using Alexa 488-labeled C2AB and either protein-free or SNARE-containing liposomes. All measurements were carried out in the presence of 150 mM KCl, 1 mM $MgCl_2$, and 3 mM ATP as in Fig. 5b. 100 μM free Ca^{2+} increased emission fluorescence of Rhodamine (**b**) and k_{obs} (s^{-1}), observed rate constants (**c**), at different C2AB concentrations. Data are mean ± SD (n = 10 – 15). a.u., arbitrary unit. Raw data of stopped-flow spectroscopy are shown in Supplementary Fig. 7e.

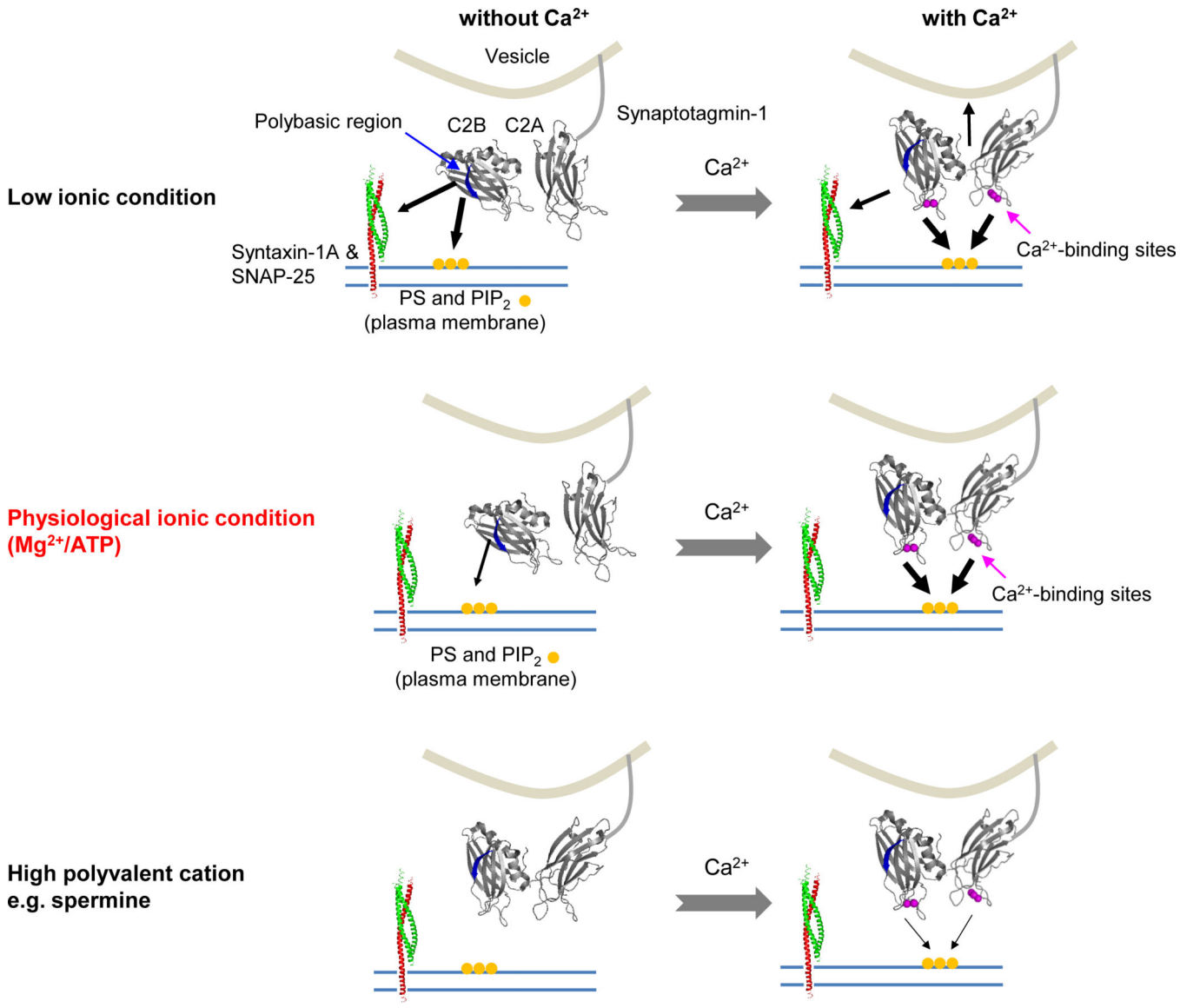

Figure 7. Cartoon summarizing the interactions of synaptotagmin-1 with SNAREs and PIP_2-containing membranes under different ionic conditions

The thickness of the arrows indicates the strength (affinity) of the interaction. Note that for clarity the PIP_2-clusters are depicted as being separated from the SNARE complexes which is likely not the case. The SNARE complexes are shown without synaptobrevin-2 for simplicity.